PERPENDICULAR ELECTRON HEATING BY ABSORPTION OF AURORAL KILOMETRIC RADIATION

by

D. D. Morgan[1], J. D. Menietti[1],

R. M. Winglee[2], and H. K. Wong[3]

April 1994
Revised September 1994

[1]Department of Physics and Astronomy, University of Iowa, Iowa City, Iowa 52242
[2]Geophysics Program AK50, University of Washington, Seattle, Washington 98195
[3]Department of Space Sciences, Southwest Research Institute, San Antonio, Texas 78228-0510

ABSTRACT

We investigate the possibility of perpendicular heating of electrons and the generation of "90°-electron conics" by particle diffusion in velocity space due to wave-particle interaction with intense auroral kilometric radiation. This interaction is made possible by the downward shift in the R-X cutoff below the electron cyclotron frequency that occurs in the presence of warm plasma. We simulate this condition and solve the diffusion equation using a finite difference algorithm. The results show strong perpendicular electron heating and indicate that the main characteristics of an electron conic distribution can be reproduced under these conditions.

I. INTRODUCTION

The term "conic" was first applied to an electron distribution by Menietti and Burch [1985] and was used to refer to electron distributions that were enhanced along the loss cone. This type of conic distribution has been associated with upper hybrid resonance waves by Wong et al. [1988], suggesting that the electron distribution can be obliquely heated by this type of wave. Menietti et al. [1993] have observed another type of conic distribution involving perpendicularly heated electron distributions, which may be called 90°-conic distributions; these distributions were observed near auroral kilometric radiation (AKR) source regions. Subsequently, Menietti et al. [1994] have hypothesized that the observed heating of electrons and the filling-in of observed loss cones is caused by particle diffusion in velocity space due to interaction with high intensity auroral kilometric radiation (AKR) (cf. their Figure 8).

Auroral kilometric radiation is commonly observed at spectral densities of up to 10^{-9} $(V/m)^2/Hz$ [Gurnett, 1974] and frequencies up to several hundred kilohertz and down to the R-X cutoff [Benson and Calvert, 1979; Gurnett et al., 1983; Bahnsen, 1989]. Benson and Calvert [1979] find that the wave normal angle is probably close to 90°. In source regions, AKR is observed to exist at frequencies below the local electron cyclotron frequency [cf. Bahnsen et al., 1989; Menietti et al., 1993]. This occurrence is due to the presence of a relativistic plasma distribution, which can drive the R-X cutoff below the electron cyclotron frequency [Winglee, 1985]. Ungstrup et al. [1990] have shown that the loss cone in the AKR source region is filled in and have hypothesized that this effect is due to fast diffusion brought about by a wave-particle interaction. In the present paper, we examine the hypothesis that fast electron diffusion due to

interaction of the electron distribution with AKR can cause the 90°-electron conic distributions observed by Dynamics Explorer, as proposed by Unstrup et al. [1990] and Menietti et al. [1994].

Wu et al. [1981] approximate the diffusion coefficient for conditions applicable to fundamental R-X mode AKR. Using this approximation, we estimate the value of the diffusion coefficient and compute representative diffusion times for various distributions. To simulate the action of diffusion on a particle distribution, a finite difference algorithm is then used to solve the diffusion equation given by Wu et al. [1981] We shall show that perpendicular electron heating can be reproduced under conditions approximating those in the AKR source region.

In Section II, we discuss some relevant observations. In Section III, we look at the phenomenon of diffusion and the effects of the form of the index of refraction and the resonant ellipse on that phenomenon. In Section IV, we simulate perpendicular diffusion due to AKR under plausible conditions and look at its effects on a model distribution function. In Section V, we draw conclusions concerning the likelihood of this mechanism.

II. OBSERVATIONS

Plate 2 of Menietti et al. [1993] shows a spectrogram of an AKR event observed at an unusually high altitude in the nightside auroral region by DE 1 on 12 October 1981. Two spacecraft positions where intense AKR emission extends below the local electron cyclotron frequency are indicated on the spectrogram, one at 00:28:30 universal time (UT) and the other at 00:29:30 UT, which Menietti et al. [1993] (cf., Bahnsen et al., 1987, 1989) conclude are source field lines. In this plate, a region is indicated between two dashed lines where strong perpendicular heating was observed. This region extends from poleward of the observed source regions to a position between the two source regions.

Figure 1 of the present paper shows a contour plot of a perpendicularly heated electron distribution occurring adjacent to and poleward of the source region observed in the aforementioned event at 00:28:30 UT. This figure shows a distinct enhancement of the electron distribution perpendicular to the magnetic field extending to about 4.5 keV. The electron distribution in the parallel direction, which we assume is unaffected by particle diffusion, extends to about 0.6 keV. There is also a clear filling in of the loss cone. We believe that the observed asymmetry and filled-in loss cone are the result of a wave-particle interaction involving intense AKR. We shall attempt to reproduce these effects by modeling the radiation spectrum, the electron distribution, and the diffusion process.

III. THE DIFFUSION COEFFICIENT, INDEX OF REFRACTION, AND RESONANT ELLIPSE

The diffusion coefficient for the case of R-X mode waves propagating nearly perpendicular to the magnetic field is given by Wu et al. [1981] as

$$D_{\perp\perp}(v_\perp, v_\parallel) = \frac{4\pi^2 e^2}{m^2} \int d^3k \; \mathcal{E}_k(t) \; \delta[\omega_r - \Omega_c/\gamma - k_\parallel v_\parallel] \tag{1}$$

where $\mathcal{E}_k(t)$ is wave energy per mode given here as a function of time, $\mathbf{k}$ is the wavevector, ω_r is the real part of the wave frequency, $\gamma = 1/\sqrt{(1 - v_\perp^2/c^2 - v_\parallel^2/c^2)}$, and Ω_c is the absolute value of the electron cyclotron frequency. For $|k_\parallel v_\parallel|/\omega_r \ll 1$, the evolution of the electron distribution function is given by the following equation from Wu et al. [1981]

$$\frac{\partial f_e}{\partial t} = \frac{1}{v_\perp} \frac{\partial}{\partial v_\perp} D(v_\perp, v_\parallel) \; v_\perp \frac{\partial f_e}{\partial v_\perp} \tag{2}$$

In this study, we do not consider the effect of the wave-particle interaction on the wave intensity, so that the wave energy per mode is considered to be constant.

Setting the argument of the delta function in Equation 1 equal to zero for a given plasma frequency, cyclotron frequency, and wave normal angle, yields the resonant ellipse, which is the locus of points in velocity space that can interact with the wave at a given frequency. Particles not on a resonant ellipse do not interact with the wave. The parameters of the resonant ellipse are given by Melrose et al. [1982] as

$$C_1 = \frac{\omega k_\parallel c}{k_\parallel^2 c^2 + (s\Omega_c)^2} \tag{3}$$

$$a = \left\{ \frac{k_\parallel^2 c^2 + (s\Omega_c)^2 - \omega^2}{k_\parallel^2 c^2 + (s^1\Omega_c)^2} \right\}^{1/2} \tag{4}$$

and

$$b = \left\{ \frac{(s\Omega_c)^2}{k_\parallel^2 c^2 + s^2\Omega_c^2} \right\} a \tag{5}$$

where C_1 is the displacement of the center of the ellipse along the $v_\parallel/c$ axis, a is the semimajor axis, and b is the semiminor axis. All parameters given here are written as a fraction of the vacuum speed of light.

Benson and Calvert [1979] determined observationally that AKR has a low-frequency cutoff at the R-X cutoff frequency. However, as mentioned above, Viking and DE 1 observations frequently show that the low-frequency cutoff of AKR can reach below the electron cyclotron frequency in the source region, indicating that the R-X cutoff has been lowered. The lowered R-X cutoff is an effect of the presence of relativistic electrons, as shown by Winglee [1985]. This effect is crucial for the existence of perpendicular electron heating by AKR.

In Figure 2 we plot the cold plasma index of refraction, in the top panel, and the square of the semimajor axis of the resonant ellipse, in the bottom panel, as a function of frequency for the following values of cyclotron frequency, plasma frequency, and wave normal angle, respectively: $f_c = 60$ kHz, $f_p = 6$ kHz, $\theta = 105°$. The R-X cutoff frequency is $f_{RX} = 60.6$ kHz; this frequency is the lower limit of the abscissa. It can be seen that the index of refraction starts at zero at the R-X cutoff and rises asymptotically toward one. The bottom panel shows

that there is a limited frequency range for which the square of the semimajor axis has positive values, starting at f = 60.8 kHz and continuing to higher frequencies. Resonant ellipses do not exist outside this frequency range for the R-X mode, at the specified plasma frequency, cyclotron frequency, and wave normal angle. Figure 3 shows several of the resonant ellipses contained in this region. Note that the size of the ellipses decreases to zero as the frequency approaches its limit at either end of this range. Note also that the area where particle diffusion is allowed is limited to the region in which the ellipses occur, to one side of the origin, as expected from Wu [1985].

Because none of the resonant ellipses contain the region where $v_{\parallel}/c \approx 0$, it is impossible to produce perpendicular heating. However, as shown in Figure 1 of Winglee [1985], the presence of warm plasma lowers the value of the R-X cutoff frequency. Equations 4 and 5 show that lowering the value of ω increases the size of the resonant ellipse. Thus it will prove useful to study the effect of lowered wave frequencies on the configuration of resonant ellipses.

A comprehensive warm plasma calculation [cf. Winglee, 1985] is beyond the scope of this paper. Therefore, in order to simulate the relativistic plasma effect on the R-X cutoff and maintain the simplicity of the cold plasma approximation, we have simply evaluated each point of the cold plasma index of refraction for a new frequency shifted downward by an arbitrary factor A times (f_{RX} - f_c), where f_{RX} is determined by cold plasma theory. Figure 4 shows that the result of this operation is a reasonable approximation to the actual warm plasma index of refraction. In this figure we replot data from Figure 1b of Winglee [1985] for a DGH distribution function with v_{Th} = 0.3c in terms of index of refraction as a function of wave frequency. We compare this result to the cold plasma index of refraction curve computed from the same plasma frequency, cyclotron frequency, and wave normal angle and new transformed

frequency until n = 0 at f = f_{RX}, evaluated from Equation A/2 of Winglee [1985]. Clearly, the two curves are similar in shape, rising abruptly from n = 0 at the cutoff and then approaching n = 1 asymptotically. The only visible difference between the two curves is that the value of $\partial n/\partial \omega$ near the cutoff is larger when calculated from the warm plasma distribution than for the frequency-shifted cold plasma distribution. This simple approximation is not rigorously correct, but it does preserve the important qualitative features of the true index of refraction and is analytically very simple.

The effect of the downward frequency shift on the allowed resonant ellipses is shown in Figures 5 and 6. Figure 5 shows, in the top panel, the index of refraction, identical to that in Figure 3, shifted downward in frequency by $2(f_{RX} - f_c)$. In the bottom panel, the effect on the square of the semimajor axis is displayed. Two effects on the resonant ellipse are obvious: first, the range in which the square of the semimajor axis is positive is extended, beginning at the new R-X cutoff frequency and extending to about the same upper limit as shown in Figure 2; second, the semimajor axis starts at a nonzero value at the R-X cutoff (f_{RX} = 59.4 kHz) and generally has much larger values than in Figure 2. The semimajor axis is seen to be nonzero at f = f_{RX}, where n = 0. The resonant ellipse corresponding to f = f_{RX} is centered on the origin, according to Equation 3. Figure 6 displays some of the ellipses in the frequency range where the square of the semimajor axis is positive, as shown in Figure 5. This simple exercise has shown that merely shifting the index of refraction to lower frequencies can cause the resonant ellipses to intersect the region surrounding the origin of velocity space, a necessary condition for a 90°-electron conic distribution to be produced.

Figure 7 shows five cuts of the function $D_{\perp\perp}(v_\perp, v_\parallel)$ for α = 1 kHz, A = 2.0, and θ = 105° for different values of $v_\parallel$. It is seen that the values of $D_{\perp\perp}$ are on the order of 10^{17}

cm^2/s^3. The sharp decrease in the value of $D_{\perp\perp}$ to zero occurs when there is no zero of the argument of the delta function in Equation 1, i.e., when

$$\Omega_c \sqrt{1-\frac{v_\perp^2}{c^2}-\frac{v_\parallel^2}{c^2}} > \omega_r - k_\parallel(\omega_r)v_\parallel \tag{6}$$

for all possible ω_r.

As shown by Figure 4, cold plasma theory yields an underestimate of the value of the value of $\partial n/\partial\omega$, implying an overestimate of the group velocity. A lower group velocity should allow the wave more time to interact with the electrons near the source region and thus result in more efficient heating of the plasma.

IV. DIFFUSION MODEL

We make two major assumptions in order to simplify the calculation of Equation 1. First, we assume that the AKR is emitted at a single wave normal angle. Here, $f_c = 60$ kHz and $f_p = 6$ kHz for all cases, similar to observed values from Menietti et al. [1993]. Energy density is given by the integral of the energy per mode, as

$$W = \epsilon_0 |E|^2 = \int d^3k \; \mathscr{E}_k \tag{7}$$

where $\mathscr{E}_k$ is the energy per mode. To describe a wave impinging on the plasma from a discrete direction, we write the energy per mode as

$$\mathscr{E}_k = \frac{1}{k^2 \sin\theta} K(k) \; \delta(\theta - \theta_0) \; \delta(\phi - \phi_0) \tag{8}$$

where K(k) is a function to be determined. The expression for the energy density becomes

$$\begin{aligned} W = \epsilon_0 |E|^2 &= \int dk \; K(k) \\ &= \int d\omega \; \frac{dk}{d\omega} \; K(k) \quad . \end{aligned} \tag{9}$$

The energy density can also be written as

$$W = \int d\omega \left[\epsilon_0 \left[\frac{d|E|^2}{d\omega} \right] \right] \quad . \tag{10}$$

By comparing the integrands of the last two equations,

$$K(k) = \frac{d\omega}{dk} \; \epsilon_0 \frac{d|E|^2}{d\omega} \quad . \tag{11}$$

By inserting this expression into Equation (1), a simple expression can be obtained for $D_{\perp\perp}$, evaluated at $\theta = \theta_0$, $\phi = \phi_0$:

$$D_{\perp\perp}(v_\perp, v_\parallel) = \frac{4\pi^2 e^2}{m^2} \int d\omega \; \epsilon_0 \frac{d|E|^2}{d\omega} \delta(\omega_r - \Omega_c / \gamma - k_\parallel v_\parallel) \quad . \tag{12}$$

The value of $d|E|^2/d\omega$ can be obtained from the power spectral density of AKR. A typical peak value of this quantity is 10^{-9} $(V/m)^2/Hz$. Since the spectral density of AKR goes to zero at $f_{R\text{-}X}$, reaches a peak, and then falls off rapidly with increasing frequency, we have approximated the spectral density by the form

$$\frac{f - f_{RX}}{\alpha} \exp\{-[\frac{f - f_{RX}}{\alpha}]^2\} \tag{13}$$

where $f > f_{RX}$ and α is a free parameter. Figure 8 shows this function for $A = 2$ for five values of α. Figure 9 shows this function for $A = 2$ and $\alpha = 200$, 500, and 1000 Hz.

The assumption of a discrete wave normal angle for AKR emission makes the computation of the diffusion coefficient by way of Equation 1 straightforward. One effect of this assumption is that there is an abrupt break between zero and nonzero values of the diffusion coefficient corresponding to the distinction between points on and not on a resonant ellipse. The discontinuity is a nonphysical result of the assumption that the radiation occurs at a single wave normal angle. We have artificially removed the sharp edge by smoothing the results.

We now show that the model assumed for the dispersion relation in the last section can be used to generate conic-like distributions for an electron population in the presence of intense AKR. We assume the electron population is physically adjacent to the AKR source region, as observed, and can be described by two components. The first component is a cold Maxwellian of energy 10 eV. The second component is a "ring distribution" with radius of v_0 and a loss cone α_{loss}. The ring distribution is calculated from the formula

$$\left[1.0 - \exp\left\{\frac{-1}{\alpha_{loss}} \sin^{-1}\left[\frac{v_\perp}{\sqrt{v_\perp^2 + v_\parallel^2}}\right]\right\}\right] \exp\left\{\frac{v_\perp^2 + v_\parallel^2 - v_0^2}{v_0^2}\right\} \qquad (14)$$

where $\alpha_{loss} = 40°$ and $v_o = 0.075$ c. A contour plot of this initial distribution is shown in Figure 9. This model does not include a relativistic population of electrons sufficient to lower the R-X cutoff significantly. According to Winglee [1985], such a distribution must have a thermal energy around 0.3c to be effective. The cool distribution shown in Figure 9 should be considered to be superimposed on the dominant relativistic plasma.

With the stated conditions, we have solved Equation 2 with a finite difference algorithm for two different sets of parameters. The time increment is $10^{-3}\ \tau_{diff}$, where τ_{diff} is given by $\tau_{diff} = v_{th}^2/D'_{\perp\perp}$, $D'_{\perp\perp}$ is taken as the value at the origin of velocity space, and v_{th} is the thermal velocity of the Maxwellian component of the unperturbed distribution function. For the first case, $\alpha = 300$ Hz, A = 1.5, and $\theta = 100°$. The result of running the finite difference computation for three diffusion times are seen in Figure 10. In comparing the result with Figure 1, we see that the Maxwellian portion of the model distribution is stretched similar to the data, although not quite as far. The loss cones are seen to fill in. In Figure 9, the sharp edge at $v_\parallel/c \simeq 0$ and at $v_\perp/c \sim 0.10$ is attributable to a sharp edge in the diffusion coefficient as discussed above.

Figure 11 shows a case with parameters $\alpha = 1$ kHz, A = 3.0, and $\theta = 105°$. The running time in this case is also three diffusion times. The Maxwellian portion of the distribution function is stretched and the loss cones filled in, similarly to Figure 10. The diffusion "edge" is not observed.

Figure 1 differs from both Figures 10 and 11 in that both the lower and higher energies of the distribution function appear to be unaffected by diffusion. We shall discuss possible reasons for this discrepancy in the final section.

V. CONCLUSIONS

This work has shown that electron diffusion due to particle interaction with strong AKR is an effective perpendicular heating mechanism for electrons. In particular, this mechanism is capable of generating "90°-electron conic" distributions on short time scales in regions adjacent to the AKR source region. The essential physics that enables this process to occur is shown in Figures 2 through 6. These figures show the effect of warm plasma in lowering the value of the R-X cutoff frequency, as discussed by Winglee [1985], enabling the resonant ellipses to encompass the origin of velocity space. Without the presence of warm plasma, the resonant ellipses would all lie to one side of the $v_\perp$ axis of velocity space, as shown by Wu [1985], and perpendicular diffusion due to AKR would have little effect on the electron distribution.

The results show a good qualitative agreement between the data and the model. In particular, we note a perpendicular stretching of the distribution function combined with some filling of the loss cone. However, we also note some significant differences between the data and the simulation. (1) The data shown in Figure 1 indicate that heating occurs most efficiently at intermediate energies, leaving low and high energy components of the distribution nearly unchanged. We were unable to recover this effect. (2) Our computation gives a sharp transition between zero and nonzero regions for the diffusion coefficient in the $v_\perp$ - $v_\parallel$ plane. This edge shows up in the simulation as a discontinuity in the evolved distribution visible in Figure 10.

Clearly, the approach to heating by diffusion undertaken here is only adequate to give a qualitative result. The weaknesses inherent in this approach are (1) use of a Maxwellian in the initial distribution since the initial distribution shown by the data is clearly non-Maxwellian;

(2) the downward frequency shift used to simulate the effect of a relativistic particle distribution; (3) the use of a simple spectral density distribution as given in Equation 9 an Figure 9; and especially (4) the use of a single wave normal angle to describe the radiation distribution. Introducing a range of wave normal angles in Equation 1 would tend to soften the sharp transition edge of the diffusion coefficient between zero and nonzero values.

Perpendicular heating of electrons due to AKR is inherently a warm plasma effect and is expected in regions adjacent to the AKR source region. The generation of 90°-electron conics near the AKR source, typically at altitudes of 3000 to 5000 km in the nightside auroral region can lead to adiabatic folding of the distribution and more typical, smaller pitch-angle, electron conics observed at higher altitudes by DE 1 [cf. Menietti et al., 1994, Figure 8].

ACKNOWLEDGEMENTS

We would like to thank Dr. I. H. Cairns for informative discussions and K. Kurth for clerical assistance. This research was supported by NASA grant NAG5-2102.

REFERENCES

Bahnsen, A., B. M. Pedersen, M. Jespersen, E. Ungstrup, L. Eliasson, J. S. Murphree, R. D. Elphinstone, L. Blomberg, G. Holmgren, and L. J. Zanetti, Viking observations at the source region of auroral kilometric radiation, J. Geophys. Res., 94, 6643, 1989.

Bahnsen, A., M. Jespersen, E. Ungstrup, and I. B. Iversen, Auroral hiss and kilometric radiation measured from the Viking satellite, Geophys. Res. Lett., 14, 471, 1987.

Benson, R. F., and W. Calvert, ISIS I observations at the source of auroral kilometric radiation, Geophys. Res. Lett., 6, 479, 1979.

Davidson, R. C., Methods in Nonlinear Plasma Theory, Academic Press, San Diego, California, 1972.

Gurnett, D. A., The Earth as a radio source: Terrestrial kilometric radiation, J. Geophys. Res., 79, 4227, 1974.

Menietti, J. D., and J. L. Burch, Electron conic signatures observed in the nightside auroral zone and over the polar cap, J. Geophys. Res., 90, (A6), 5345-5353, 1985.

Menietti, J. D., C. S. Lin, H. K. Wong, A. Bahnsen, and D. A. Gurnett, Association of electron conical distributions with upper hybrid waves, J. Geophys. Res., 97, (A2), 1353-1361, 1992.

Menietti, J. D., J. L. Burch, R. M. Winglee, and D. A. Gurnett, DE 1 particle and wave observations In auroral kilometric radiation (AKR) source regions, J. Geophys. Res., 98, 5865, 1993.

Menietti, J. D., D. R. Weimer, M. Andre, and L. Eliasson, DE 1 and Viking observations associated with electron conical distributions, J. Geophys. Res., in press, 1994.

Melrose, D. B., K. G. Rönnmark, and R. G. Hewitt, Terrestrial kilometric radiation: The cyclotron theory, J. Geophys. Res., 87, 5140, 1982.

Ungstrup, E., A. Bahnsen, H. K. Wong, M. Andre, and L. Matson, Energy source and generation mechanism for auroral kilometric radiation, J. Geophys. Res., 95, (A5), 5973-5981, 1990.

Winglee, R. M., Effects of a finite plasma temperature on electron cyclotron maser emission, Astrophys. J., 291, 160, 1985.

Wong, H. K., J. D. Menietti, C. S. Lin, and J. L. Burch, Generation of electron conical distributions by upper hybrid waves in the earth's polar region, J. Geophys. Res., 93, 10,025, 1988.

Wu, C. S., Kinetic cyclotron and synchrotron maser instabilities: radio emission processes by direct amplification of radiation, Space Sci. Rev., 41, 215, 1985.

Wu, C. S., S. T. Tsai, M. J. Xu, and J. W. Shen, Saturation and energy-conversion efficiency of auroral kilometric radiation, Astrophys. J., 248, 384, 1981.

Figure Captions

Figure 1. Contour plot of the electron distribution function on day 285 at 00:28:04 UT, poleward of an AKR source region. This contour shows perpendicular heating of the low temperature distribution out to about 4.5 keV. (From Menietti et al. [1993].)

Figure 2. (Top) The cold plasma index of refraction plotted against frequency for $\Theta_0 = 105°$, $f_{ce} = 60$ kHz, and $f_{pe} = 6$ kHz. The lower frequency limit, about 60.59 kHz, is the R-X cutoff. (Bottom) The corresponding values of the square of the semimajor axis of the resonant ellipse plotted against frequency. This figure shows that there is a limited range of frequencies in which the resonant ellipse exists.

Figure 3. Resonant ellipses corresponding to the region of positive semimajor axis squared shown in the previous figure. Note that the range of $v_{\|}/c$ is from -0.1 to -0.3. Thus, none of these ellipses encompass the origin.

Figure 4. Comparison of a numerically calculated warm plasma index of refraction, from Winglee [1985], for a DGH distribution with $\alpha = 1$, $v_{Th} = 0.3c$, $\Omega_c = 60$ kHz, $\omega_p = 27$ kHz , and $\Theta = 80°$ with a cold plasma distribution function of the same Ω_c, ω_p, and Θ transposed downward in frequency so that the cutoffs coincide.

Figure 5. (Top) Index of refraction, identical to that shown in Figure 2 but transposed downward in frequency so that the R-X cutoff is below the electron cyclotron frequency. (Bottom) Square of the semimajor of the resonant ellipse for the

index of refraction shown in the top panel. Compare with the bottom panel of Figure 2 to see how the transposition of the index of refraction downward in frequency changes the value of this quantity.

Figure 6. Resonant ellipses corresponding to the region of positive semimajor axis shown in the previous figure.

Figure 7. Values of $D_{\perp\perp}(v_\perp, v_\parallel)$ as calculated from Equation 1 for fixed values of $v_\parallel$. Plasma parameters are f_p = 6 kHz, f_c = 60 kHz and wave normal angle 105°. The distortion parameter is A = 2.0 and the spectral width α = 300 Hz.

Figure 8. The function, given in Equation 14, used to model the power spectrum of AKR. The modeling is done for five values of α.

Figure 9. The initial distribution function used for the simulation run. This initial distribution consists of a Maxwellian of thermal energy 10 eV added to a ring distribution of the form given in Equation 7 with v_o = 0.075c and α_{loss} = 40°.

Figure 10. The result of evolution of the initial distribution function shown in the previous figure after evolution for $3\tau_{diff}$, where τ_{diff} = 0.27 s. The maximum of the $v_\perp$ scale is approximately the same as that in Figure 1. In this simulation, α = 300 Hz, A = 1.5, and θ = 100°.

Figure 11. Same as Figure 9 but for α = 1000 Hz, A = 3.0, and θ = 105°. The evolution time is approximately $3\tau_{diff}$, where τ_{diff} = 0.34 s.

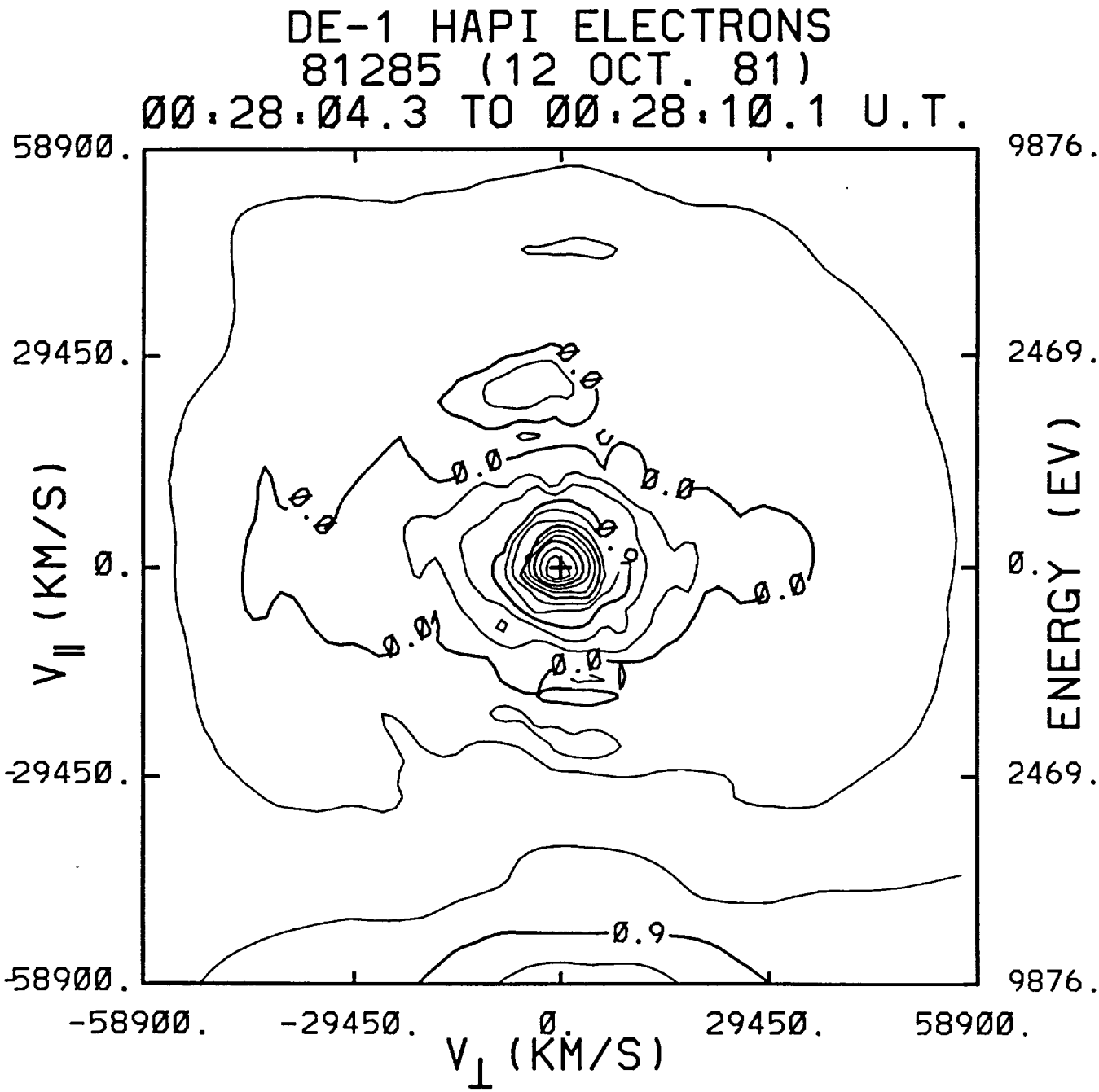
DE-1 HAPI ELECTRONS
81285 (12 OCT. 81)
00:28:04.3 TO 00:28:10.1 U.T.
58900.
29450.
0.
-29450.
-58900.
9876.
2469.
0.
2469.
9876.
$V_{\parallel}$ (KM/S)
ENERGY (EV)
0.0
0.9
-58900.
-29450.
0.
29450.
58900.
$V_{\perp}$ (KM/S)
CONTOUR INCREMENT 0.3
CONTOUR FROM -1.2 TO 3.3

Fig. 1

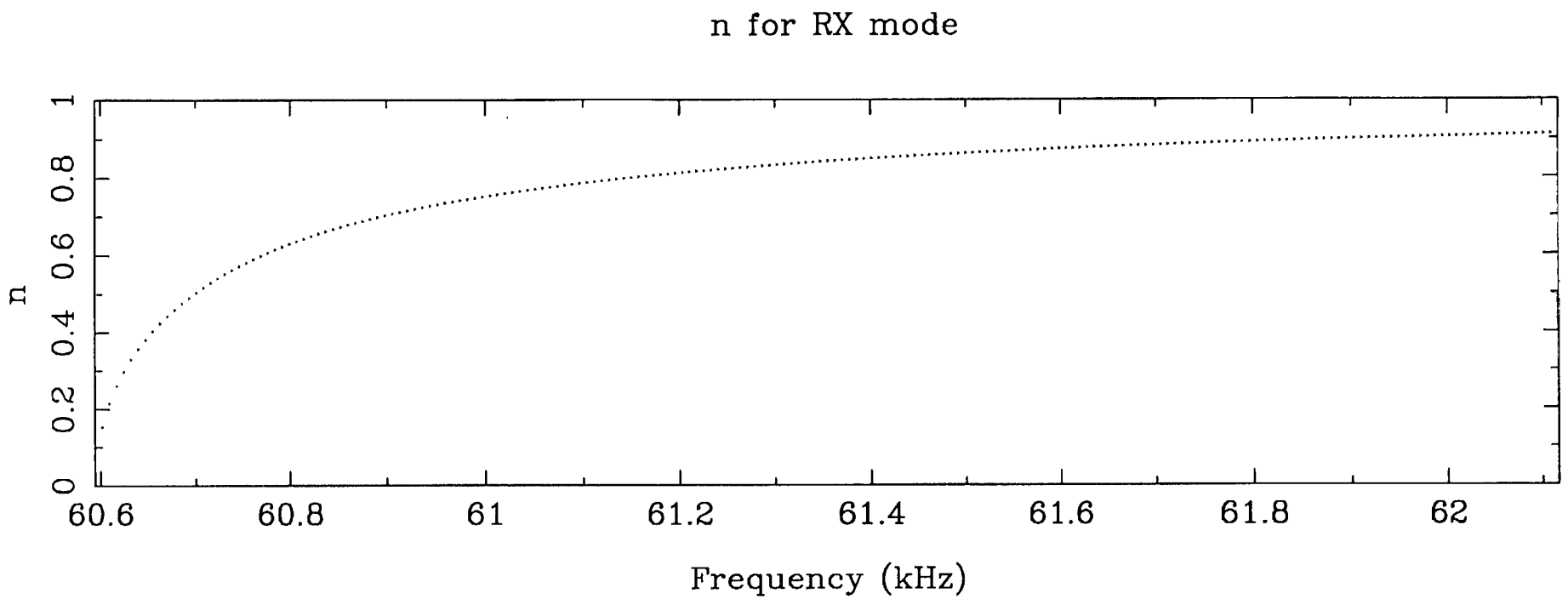
n for RX mode
n
0
0.2
0.4
0.6
0.8
1
60.6
60.8
61
61.2
61.4
61.6
61.8
62
Frequency (kHz)

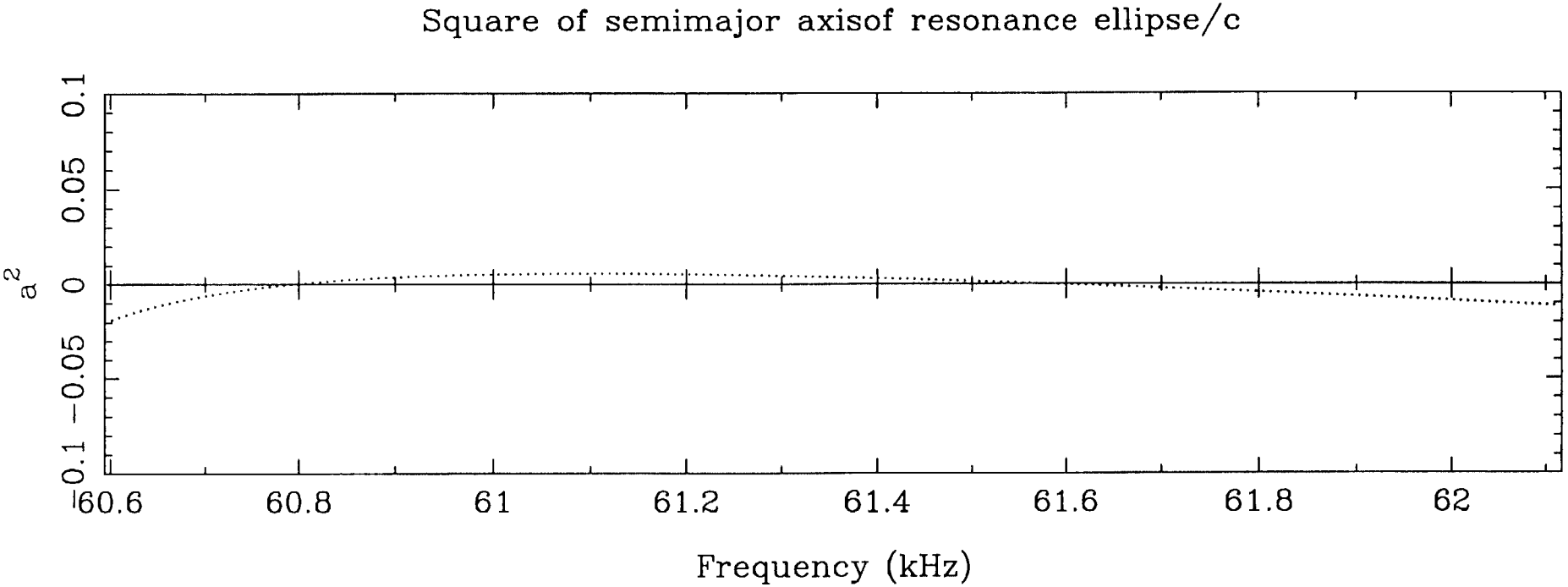
Square of semimajor axisof resonance ellipse/c
a^2
0.1
0.05
0
−0.05
−0.1
60.6
60.8
61
61.2
61.4
61.6
61.8
62
Frequency (kHz)

Fig. 2

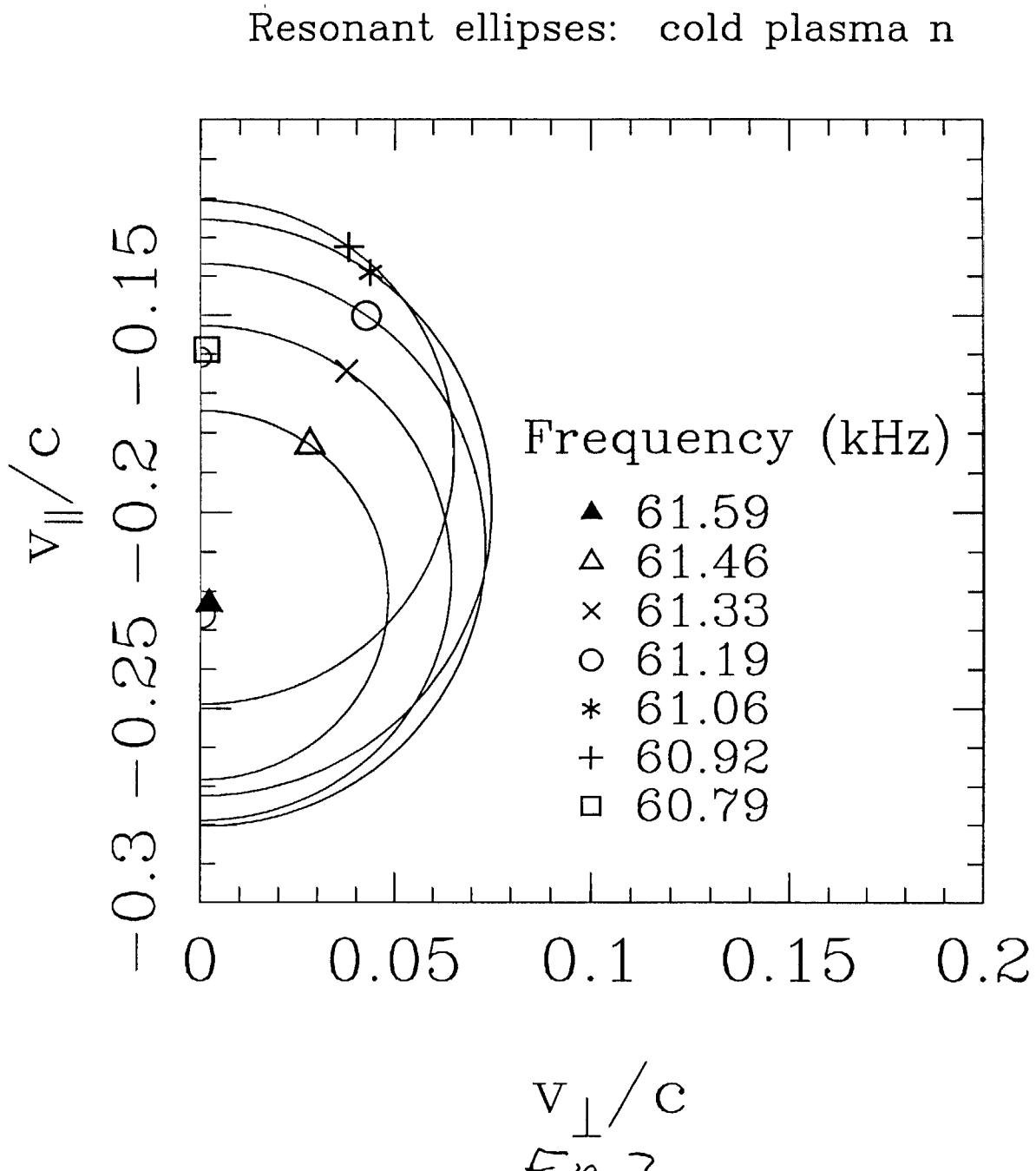
Resonant ellipses: cold plasma n
Frequency (kHz)
61.59
61.46
61.33
61.19
61.06
60.92
60.79
$v_{\parallel}/c$
$v_{\perp}/c$
−0.3
−0.25
−0.2
−0.15
0
0.05
0.1
0.15
0.2

Fig. 3

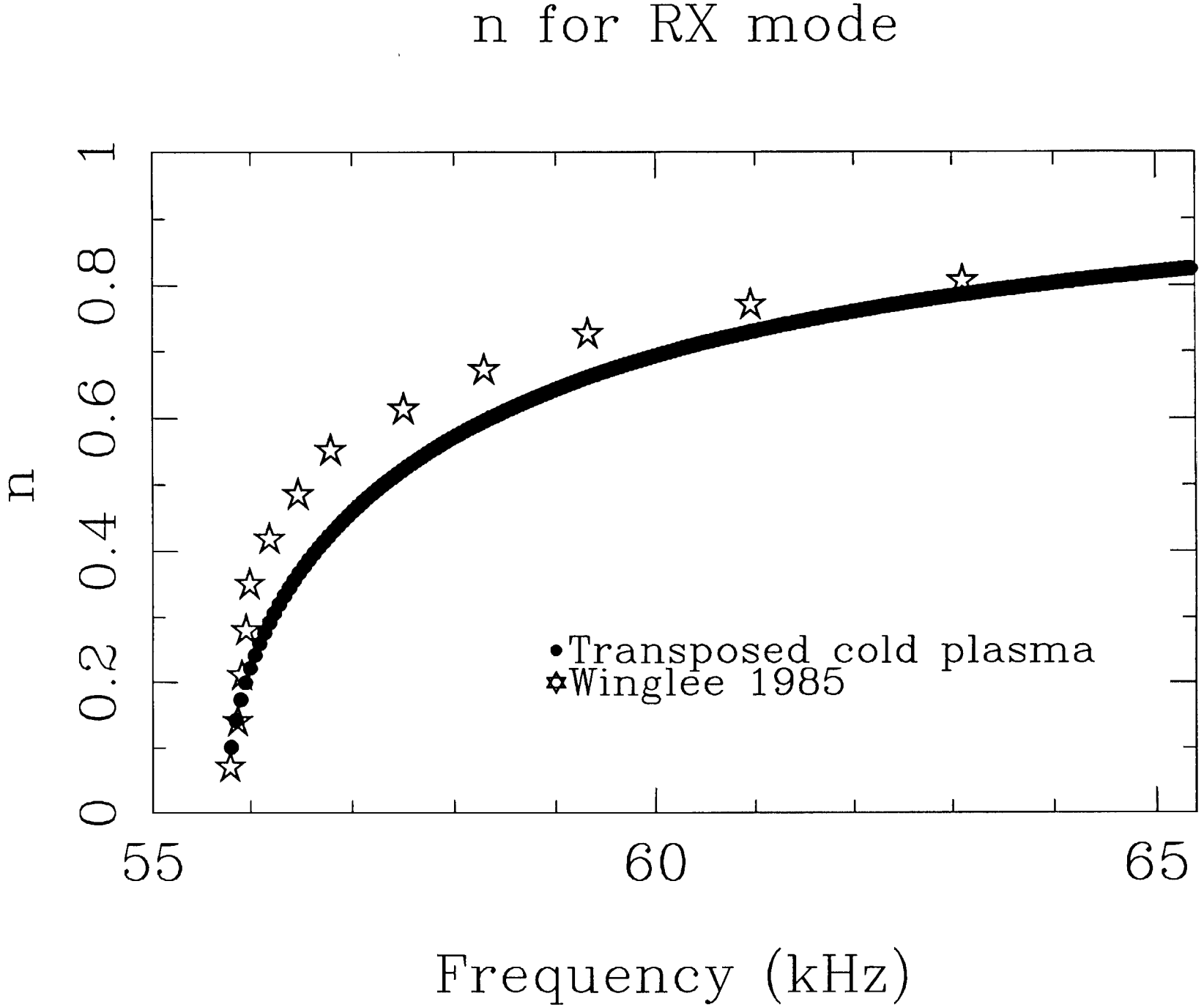
n for RX mode
n
0
0.2
0.4
0.6
0.8
1
55
60
65
Frequency (kHz)
•Transposed cold plasma
✡Winglee 1985

Fig. 4

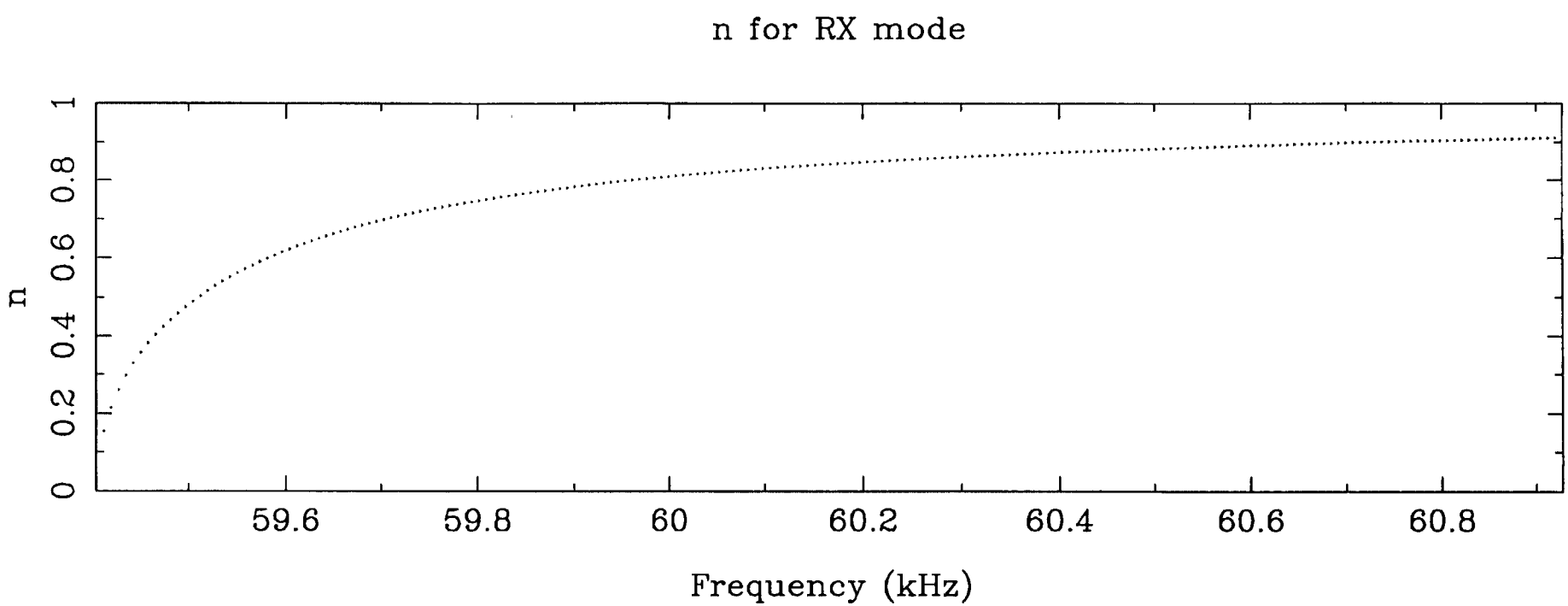
n for RX mode
n
0
0.2
0.4
0.6
0.8
1
59.6
59.8
60
60.2
60.4
60.6
60.8
Frequency (kHz)

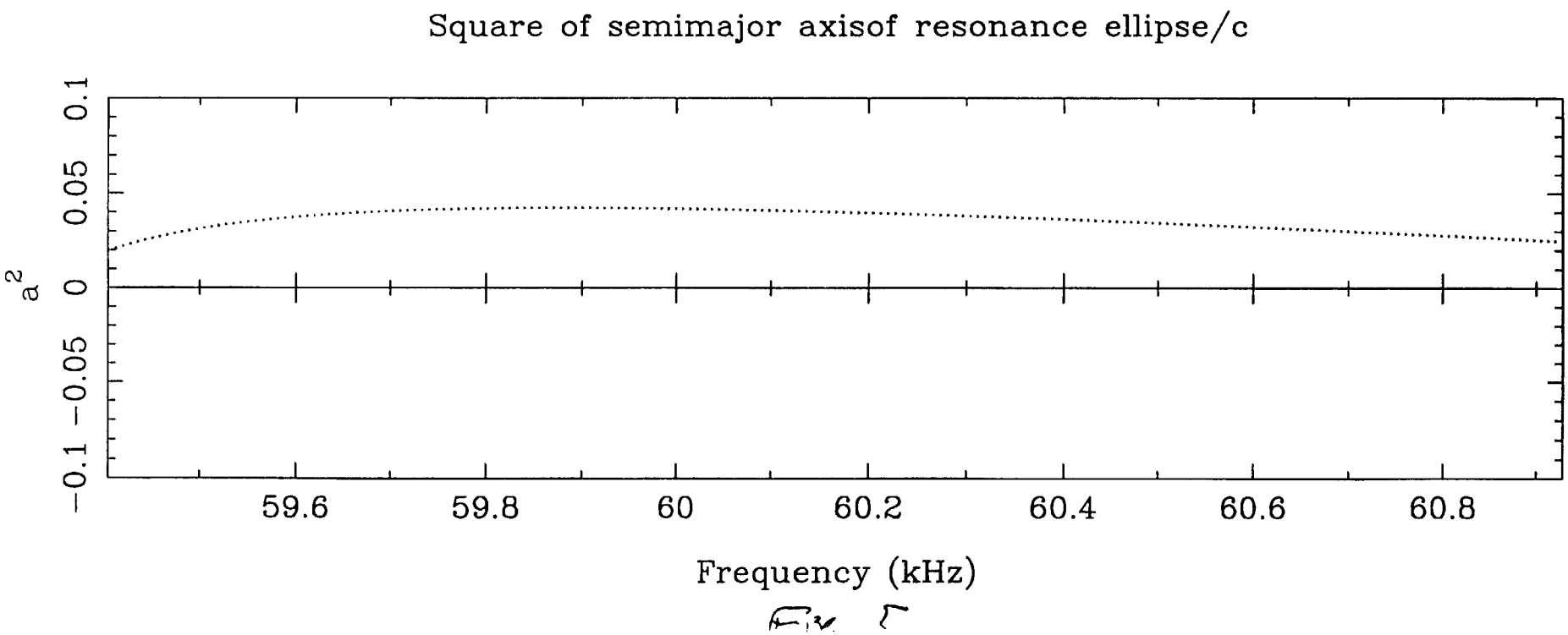
Square of semimajor axisof resonance ellipse/c
a^2
0.1
0.05
0
−0.05
−0.1
59.6
59.8
60
60.2
60.4
60.6
60.8
Frequency (kHz)

Fig 5

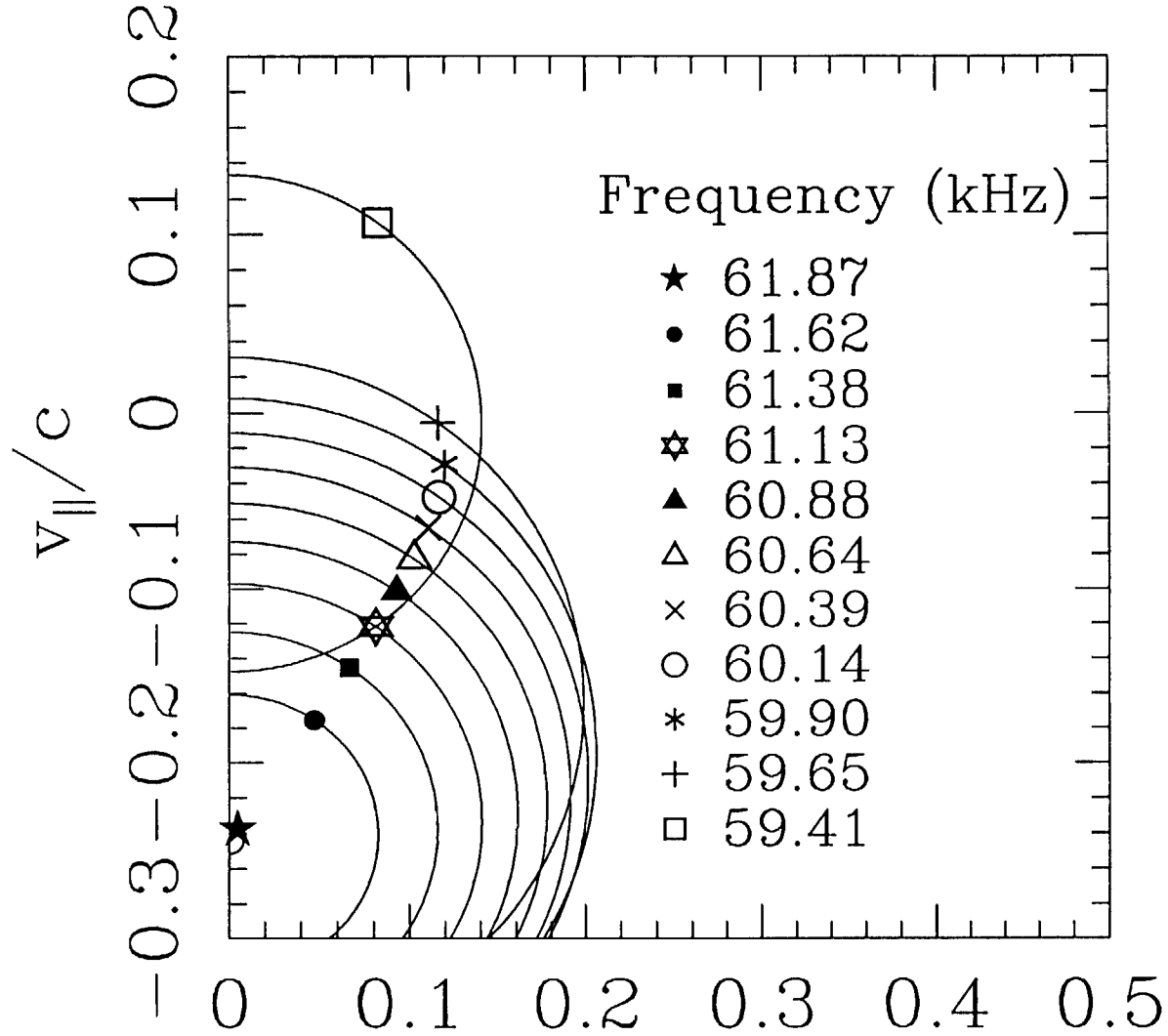
Resonant ellipses: transposed cold plasma n
Frequency (kHz)
61.87
61.62
61.38
61.13
60.88
60.64
60.39
60.14
59.90
59.65
59.41
$v_{\parallel}/c$
$v_{\perp}/c$
0.2
0.1
0
−0.1
−0.2
−0.3
0.1
0.2
0.3
0.4
0.5

Fig. 6

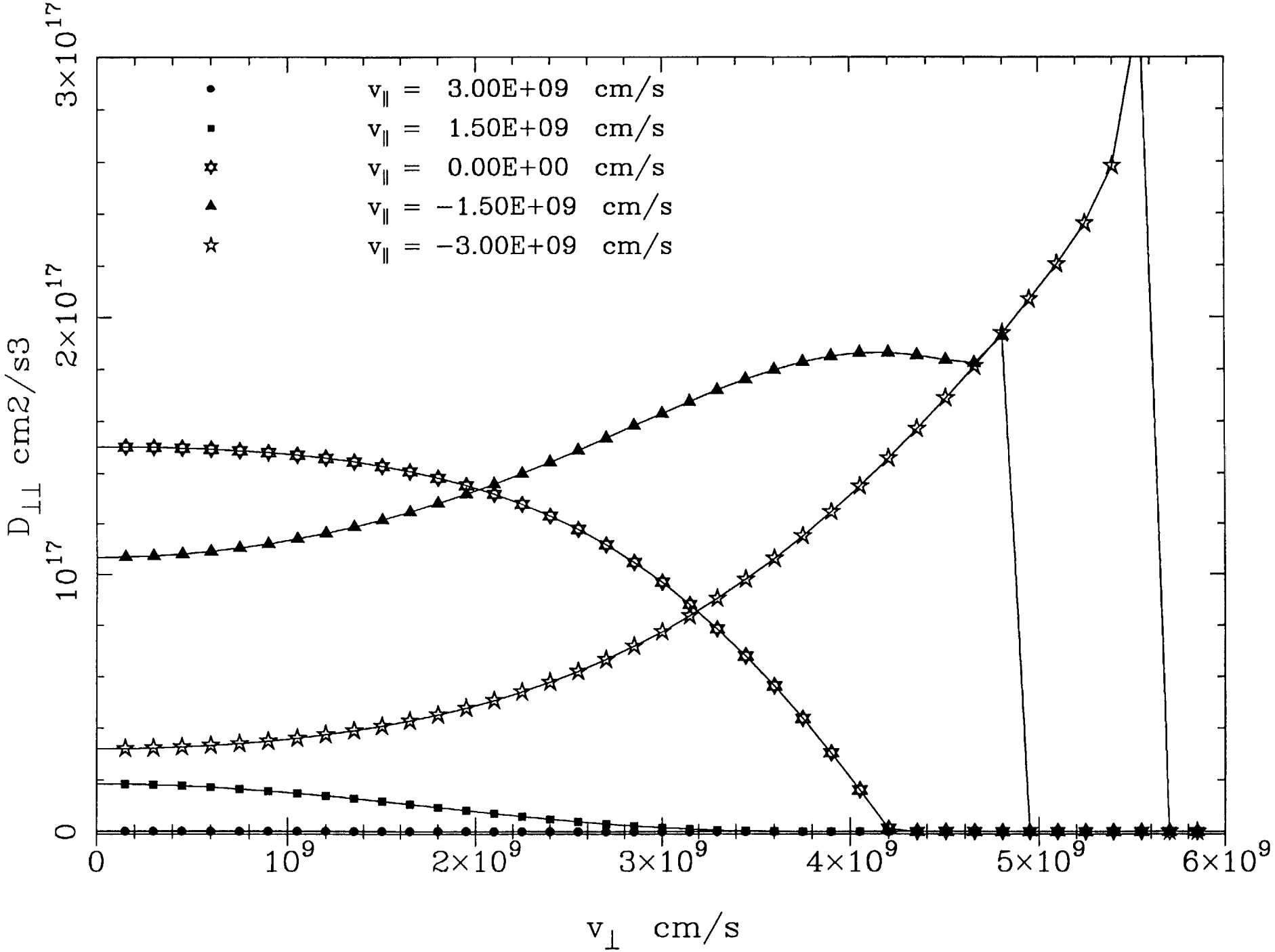
Diffusion coefficient as a function of v
$v_{\parallel}$ = 3.00E+09 cm/s
$v_{\parallel}$ = 1.50E+09 cm/s
$v_{\parallel}$ = 0.00E+00 cm/s
$v_{\parallel}$ = −1.50E+09 cm/s
$v_{\parallel}$ = −3.00E+09 cm/s
$D_{\perp\perp}$ cm2/s3
0
10^{17}
2×10^{17}
3×10^{17}
0
10^{9}
2×10^{9}
3×10^{9}
4×10^{9}
5×10^{9}
6×10^{9}
$v_{\perp}$ cm/s

Fig. 7.

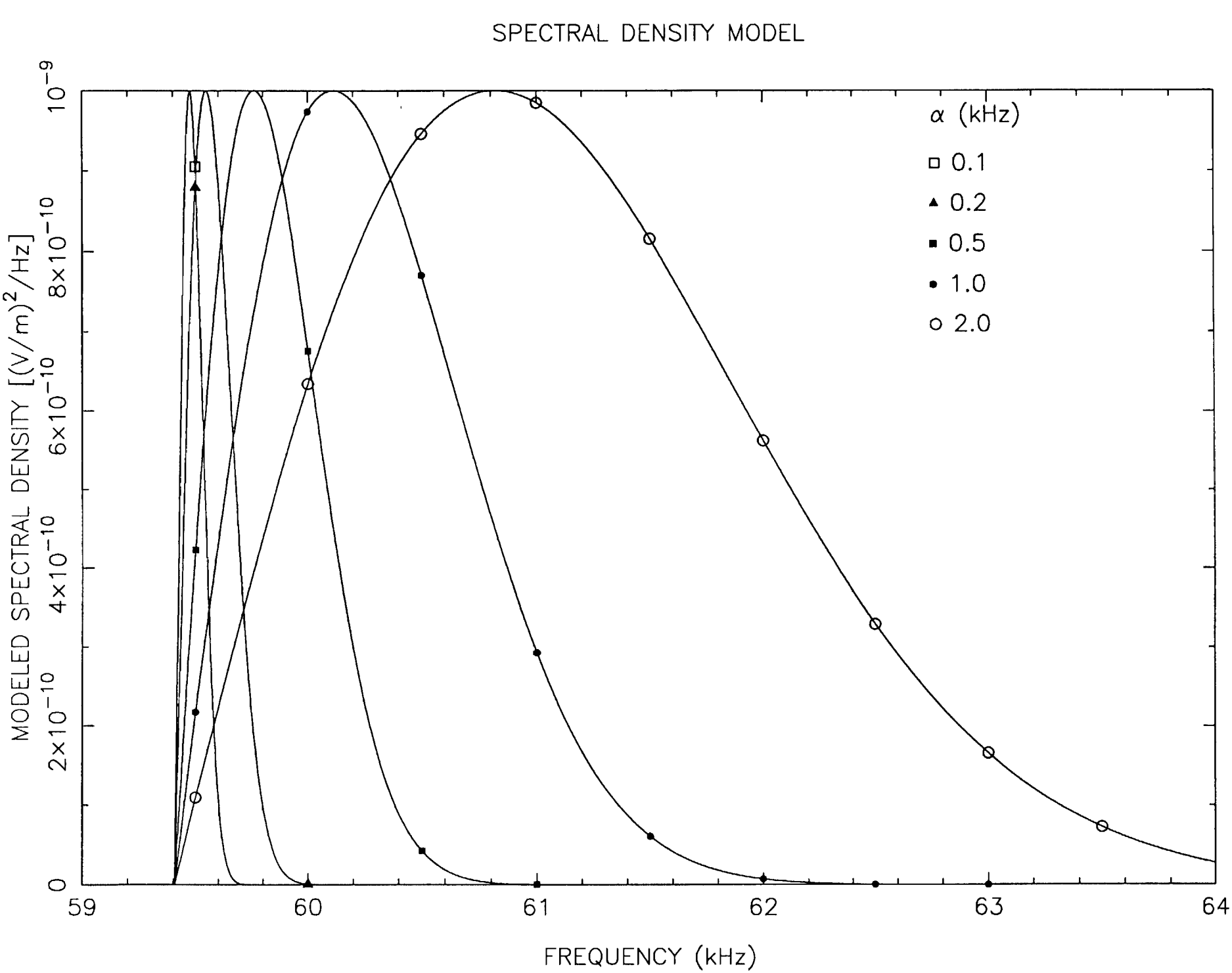
SPECTRAL DENSITY MODEL
MODELED SPECTRAL DENSITY [(V/m)^2/Hz]
0
2x10^{-10}
4x10^{-10}
6x10^{-10}
8x10^{-10}
10^{-9}
59
60
61
62
63
64
FREQUENCY (kHz)
α (kHz)
0.1
0.2
0.5
1.0
2.0

FIG 8.

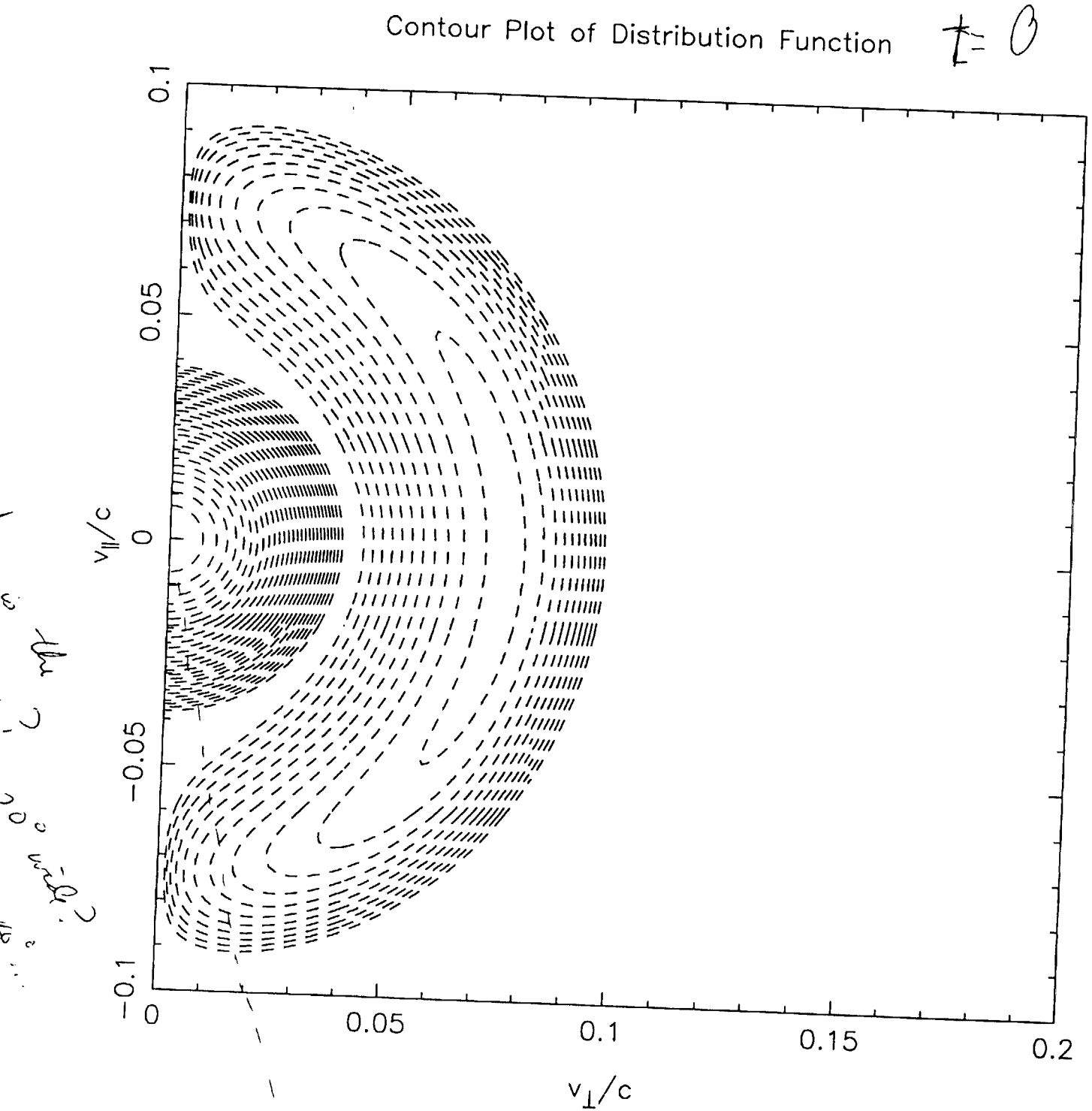
Contour Plot of Distribution Function
t = 0
0.1
0.05
0
−0.05
−0.1
$v_{\parallel}/c$
0
0.05
0.1
0.15
0.2
$v_{\perp}/c$

Fig. 9

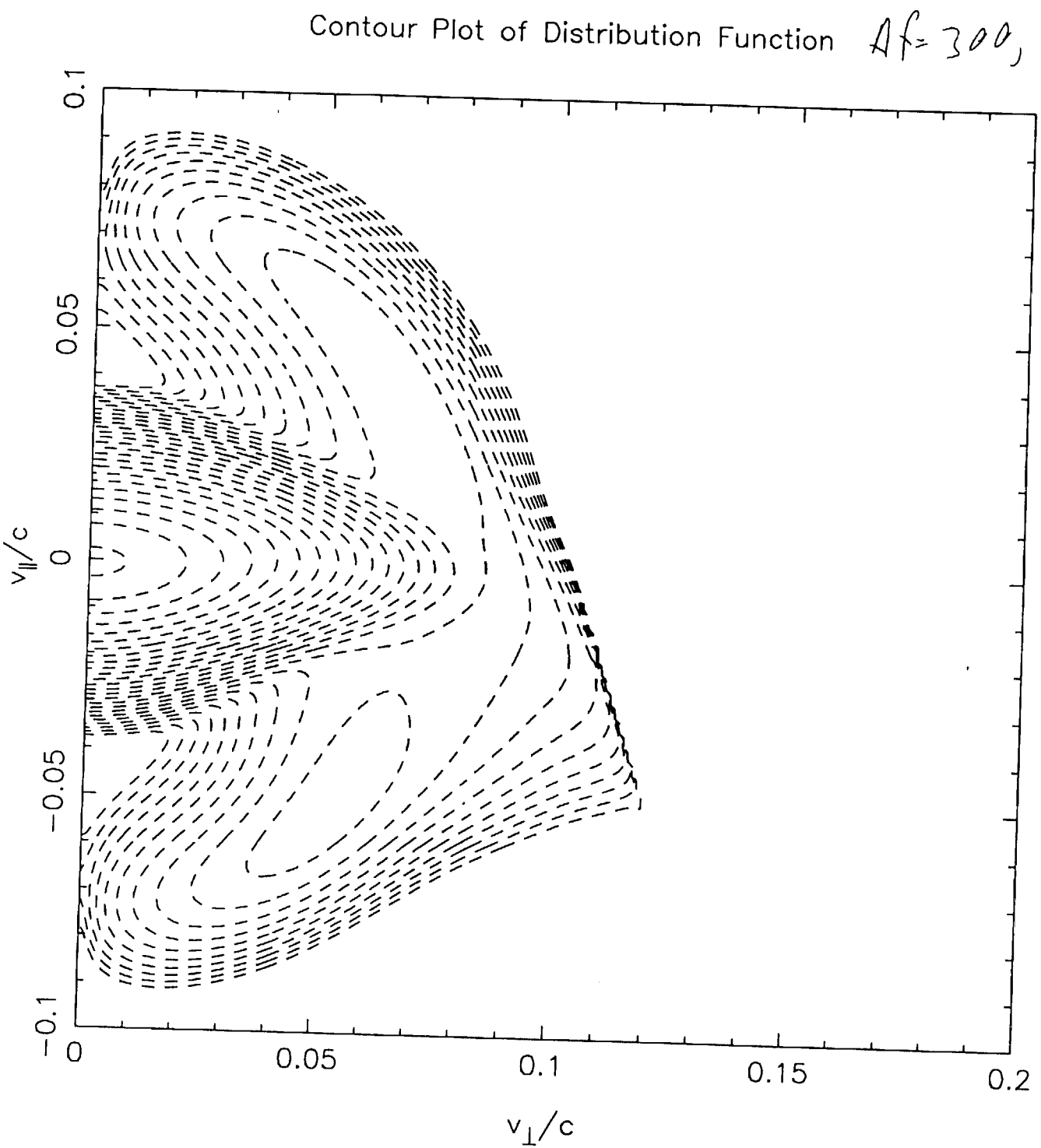
Contour Plot of Distribution Function Af=300, ff=1.5, θ=100
t=3
0.1
0.05
0
−0.05
−0.1
$v_{\parallel}/c$
0
0.05
0.1
0.15
0.2
$v_{\perp}/c$

Fig #10

Contour Plot of Distribution Function $\Delta f = 1000$, $ff =$

$t =$

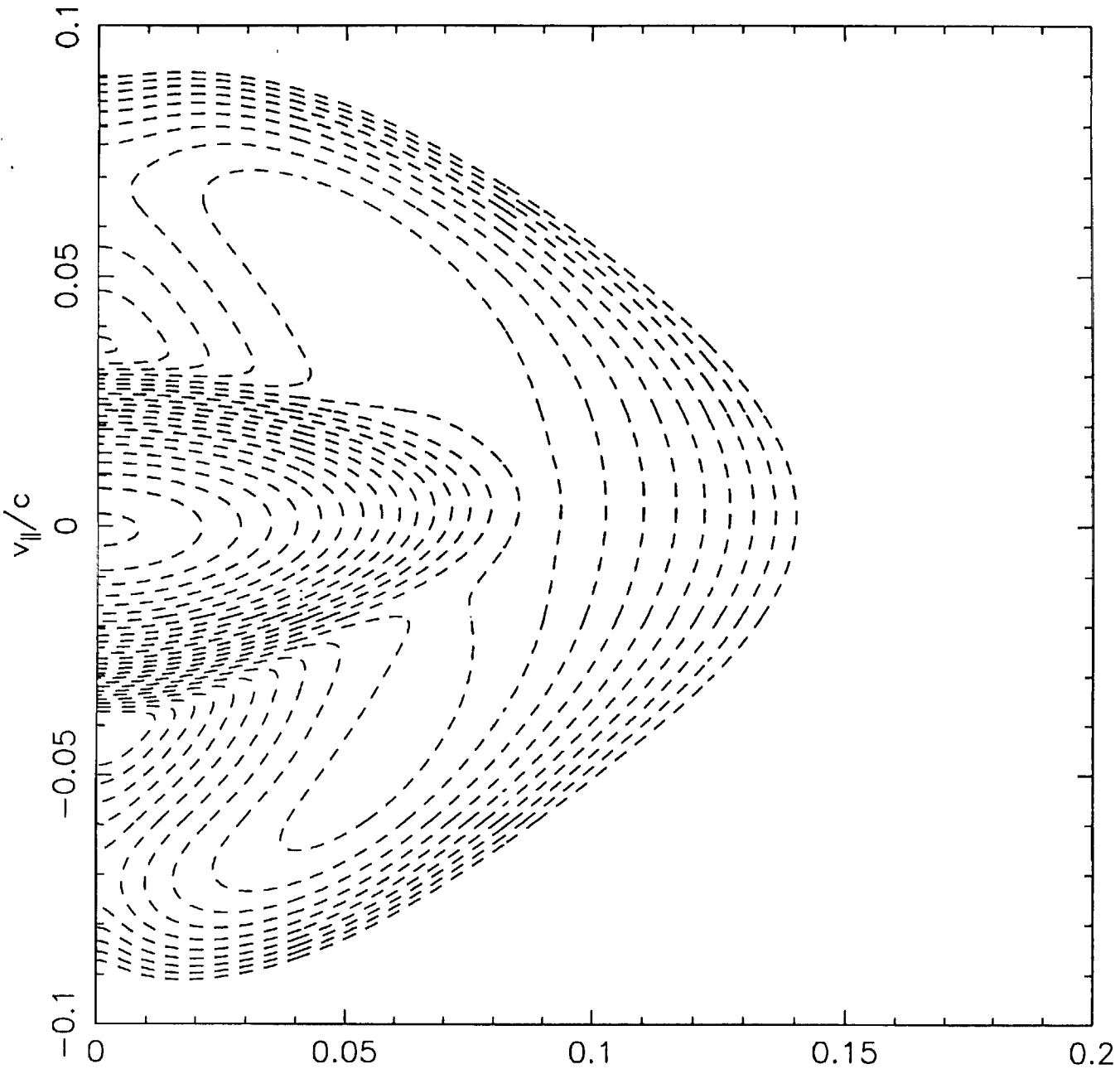

Fig. 11